Synthesis of TiO₂–ZrO₂ Mixed Oxides via the Alginate Route: Application in the Ru Catalytic Hydrogenation of Levulinic Acid to Gamma-Valerolactone

Agnieszka M. Ruppert [1],* [ID], Pierre Agulhon [2], Jacek Grams [1] [ID], Malgorzata Wąchała [1], Joanna Wojciechowska [1], Dariusz Świerczyński [2], Thomas Cacciaguerra [2], Nathalie Tanchoux [2] [ID] and Francoise Quignard [2]

1   Institute of General and Ecological Chemistry, Faculty of Chemistry, Lodz University of Technology, Żeromskiego 116, 90-924 Łódź, Poland; jacek.grams@p.lodz.pl (J.G.); malgorzata.chelmicka@gmail.com (M.W.); ms.joanna.wojciechowska@gmail.com (J.W.)
2   Institute Charles Gerhardt Montpellier, Matériaux Avancés pour la Catalyse et la Santé UMR 5253, Univ. Montpellier, CNRS, ENSCM, 240 avenue du Professeur Emile Jeanbrau-34296 Montpellier CEDEX 5, France; pierre.agulhon@enscm.fr (P.A.); dariusz.swierczynski@enscm.fr (D.Ś.); Thomas.Cacciaguerra@enscm.fr (T.C.); nathalie.tanchoux@enscm.fr (N.T.); francoise.quignard@enscm.fr (F.Q.)
*   Correspondence: agnieszka.ruppert@p.lodz.pl

Abstract: In this work, high surface area mono- and binary oxide materials based on zirconia and titania synthetized via the alginate route were applied as supports of ruthenium catalysts used in levulinic acid hydrogenation towards γ–valerolactone. The physicochemical properties of the catalysts were investigated using surface (like time-of-flight secondary ion mass spectrometry (ToF-SIMS), transmission electron microscopy (TEM)) and bulk techniques (temperature-programmed reduction (TPR), X-ray diffraction (XRD)). The obtained results exhibited that the proposed synthesis method allows for modification of the shape, morphology, and surface properties of the studied materials. These catalysts were tested in levulinic acid hydrogenation, in which catalytic support is known to be crucial. The results revealed that the titania-supported catalyst was the most active in the reaction mentioned above, while the highest mechanical stability was observed for zirconia-supported materials.

Keywords: alginate synthesis route; TiO₂–ZrO₂; Ru catalysts; biomass; gamma-valerolactone; levulinic acid

1. Introduction

The development of new synthetic routes to mono- and mixed metal oxides to improve the textural, structural crystalline phase properties of such materials, especially considering their use as catalysts, is always highly desirable. Therefore, an alternative synthesis pathway for oxides such as TiO₂ or ZrO₂ would be extremely interesting. Due to their versatile properties (like reducibility, moderate acidity, stability) they have many possible applications in heterogeneous catalysis [1].

Such materials can be synthesized by different methods, however a biomass-derived catalyst would be superior as it is a sustainable. Algae are considered the third generation of biomass. Alginates, natural polysaccharides distributed widely in the cell walls of brown macro algae, can be used as one of the precursors of catalyst supports in this case. They consist of linear block copolymers based on α-L-guluronate and β-D-mannuronate monomers (respectively named as G and M units) (Scheme 1).
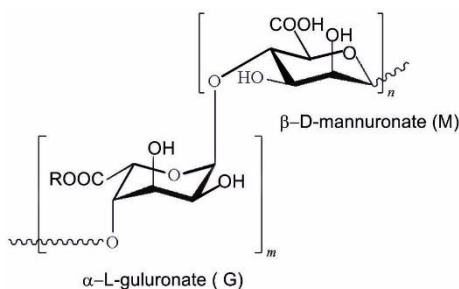
Scheme 1. Structure of alginate (M—mannuronate unit; G—guluronate unit), where R is Ca (calcium alginate) or Na (sodium alginate).

Alginates are considered very interesting materials, not only due to their low cost but especially thanks to their variable properties. In the presence of cations they can form hydrogels according to a complexation mechanism. After adding a divalent cation such as Ca^{2+}, Zn^{2+} Ba^{2+}, or Cu^{2+}, we have already shown that sodium alginate can easily transform into a stable hydrogel [2,3].

Properties of the hydrogel depend on the nature of both the alginate and transition metal cations used in excess [4]. Controlled conditions of ion exchange allow designing heterocationic materials of the desired composition. After calcination of such materials, it is possible to obtain, for example, oxides with large surface areas that can be used as catalysts or supports for catalysts [3,5,6]. This process is able to produce oxides with peculiar properties [7,8]. It gives the opportunity for the design of catalysts tailored to certain processes and additionally helps in future commercialization of such catalytic materials, as desired shapes of grains can be obtained. In the particular case of zirconia, we already showed in a previous work that we were able, by this synthesis pathway, to modulate the phase and surface properties of pure ZrO_2 [8].

Taking that into account, we decided to develop an alginate route for the synthesis of mixed TiO_2–ZrO_2 binary oxides in order to improve their catalytic performance in novel, industrially important sustainable processes. The field of biomass valorization should be highlighted among titania and zirconia applications as catalysts supports. Particular interest was found for hydrogenation reactions of biomass delivered platform molecules like levulinic acid (LA), which can be obtained from lignocellulosic biomass via hydrolysis. Hydrogenation of levulinic acid towards γ–valerolactone (GVL)—possible fuel additive, green solvent, and precursor for fuels and bulk polymers—requires metal-supported catalysts. Ru is the metal of choice of LA hydrogenation when the reaction is performed in water as a solvent and under external hydrogen pressure [9]. On the other hand, it is known that the choice of different supports can significantly influence the activity of ruthenium [10].

Concerning the literature, there are the examples proving that zirconia or titania are the most optimum ruthenium supports for this reaction. On one hand, Tan et al. concluded that titania is the most suitable as a Ru support as the strong interaction between Ru and TiO_2 facilitates the dispersion of metal and therefore increases the stability of the catalyst [11]. This behavior was confirmed later on in the recent study of Piskun et al. [12]. We showed that different titania properties can strongly influence the activity of LA hydrogenation. Rutile containing titania gives the best catalytic performance for Ru catalysts due to the fact that it has the highest dispersion of metal in contrast to anatase-based titania, where large metal clusters were formed [13].

On the other hand, several works showed predominance of zirconia vs. titania as a Ru support [14,15]. This behavior is mainly related with the high stability of zirconia materials and resistance to carbon deposit formation. In contrast, titania materials can be poisoned by the biomass or reaction origin impurities (like H_2SO_4) [16]. The preparation method of zirconia materials, however strongly, influences the activity, which was shown in hydrolytic hydrogenation of cellulose to GVL [17]. Such high stability of zirconia was also shown in the work of Futon et al., where the authors proved that Ru/ZrO_2 applied for LA hydrogenation in dioxan was more efficient that Ru/TiO_2 in terms of high mechanical and thermal stability. The Ru/TiO_2 was deactivated to a the higher degree after the catalytic

cycle in comparison to Ru/ZrO$_2$. This was mainly due to instability of the support and encapsulation of the Ru nanoparticles due to the presence of a strong SMSI effect [14].

In this work, we prepared a series of titania and zirconia binary metal oxides obtained from alginate hydrogels and tested these materials as catalyst supports of Ru catalysts in the hydrogenation of levulinic acid. To the best of our knowledge, work concerning the synthesis of zirconia–titania oxides from alginate hydrogel, as well as their use in γ-valerolactone formation, has not been described in the literature yet. We concentrated on the influence of the synthesis conditions on the structural properties of those materials, and their catalytic activity. We showed that application of alginate route for the synthesis of the supports allowed for the modification of the morphology and shape of the prepared catalysts.

2. Experimental

2.1. Preparation of the Oxides from Alginate Hydrogel Solution

In each case, in the first step the hydrogel solution of 2% *w/w* sodium alginate (PROTANAL LF 200S containing 65–75% of guluronic polymer) was prepared in deionized water.

Then, in the case of TiO$_2$ and ZrO$_2$, such prepared alginate solution was added dropwise using a syringe with a 0.8 mm diameter needle at room temperature during stirring to 0.1 mol·L^{-1} solutions of the respective salts' titanium (IV) oxysulfate hydrate (Sigma-Aldrich, France) TiOSO$_4$ ·H$_2$O or zirconyl chloride octahydrate, >99.0 pure, FLUKA. Millimetric microspheres of gel were thus formed, which were kept under stirring in this solution for 18 h, after this time they were separated from the cationic solution and washed with distilled water. The hydrogel microspheres were then immersed in a sequence of ethanol–water baths of increasing alcohol concentration (10%, 30%, 50%, 70%, 90%, and 100%), each lasting 30 min. Then the samples were dried at 40 °C under reduced pressure and calcined at 450 °C with the ramp of 3 °C/min for 7 h in static air.

In the case of mixed oxides, both the alginate solution and microspheres were prepared in the way described above. The modifications were related to the next step of cation introduction:

(a) For ZR-1, the hydrogel was obtained by gelification in an equimolar mixture of both precursors and kept in this mixture for 18 h;

(b) For ZR-2, the hydrogel was firstly formed in the titanium (IV) solution for 18 h, then washed in deionized water and introduced to the zirconium solution (with a concentration corresponding to half of the titanium atoms) for 18 h; the following procedures were identical to those described above;

(c) For ZR-3, the hydrogel was firstly formed in the zirconium solution for 18 h, then washed in deionized water and introduced to the titanium solution (with a concentration corresponding to half of the zirconium atoms) for 18 h; the following procedures were identical to those described above.

2.2. Catalyst Preparation

All samples were impregnated with 5% ruthenium from methanolic solution of Ru(acac)$_3$ (Sigma–Aldrich, France, 97%), dried at 120 °C overnight, calcined at 200 °C in static air, and reduced at 200 °C in a flow of hydrogen for 1 h. The ruthenium content in the catalysts was determined by inductively coupled plasma optical emission spectroscopy (ICP-OES). The Ru content in all catalysts was 4.9 ± 0.2 wt.%.

2.3. Catalyst Characterization

Temperature-programmed reduction (TPR) was performed on an AMI1 system from Altamira Instruments (USA) equipped with a thermal conductivity detector (TCD) and was used for examining the reducibility of catalysts. Catalysts were tested after the calcination procedure, before the measurement catalysts were preheated at 200 °C in the flow of 2 vol % O$_2$ and 98 vol % Ar for

30 min. In the measurements, a mixture of 5 vol.% H_2 and 95 vol.% Ar was used with the temperature ramp of 10 °C/min.

Time-of-flight secondary ion mass spectrometry (ToF-SIMS) was applied to the investigation of the surface composition of the catalysts. Secondary ion mass spectra were recorded with a ToF-SIMS IV mass spectrometer manufactured by ION-TOF GmbH, Muenster, Germany. Bi_3^+ was used as the primary ion source. The analysis area of sample surface was 500 μm × 500 μm. Secondary ions emitted from the bombarded surface were mass separated and counted in a high mass resolution time-of-flight (ToF) analyzer. During analysis, a pulsed low-energy electron flood gun was used for charge neutralization.

X-ray diffraction (XRD) measurements were carried out using a PANalytical X'Pert Pro MPD diffractometer. The X-ray source was a copper long fine focus X-ray diffraction tube operating at 40 kV and 30 mA. Data were collected in the 10–80° range with 0.0167° step. Crystalline phases were identified by references to the ICDD PDF-2 (ver. 2004) database. All calculations were performed with the X'Pert HighScore Plus computer program. Samples before the measurements were crushed.

Scanning electron microscopy with energy dispersive spectroscopy (SEM-EDS) measurements were performed using a S-4700 scanning electron microscope produced by HITACHI (Japan), equipped with an energy dispersive spectrometer from Thermo Noran (USA).

Brunauer–Emmett–Teller (BET) surface area and porosimetry measurements were carried out on an ASAP2010 Micromeritics using N_2 as adsorbent at −196 °C, with a prior outgassing of the samples at 200 °C for 3 h in order to desorb the impurities or moisture. The BET specific surface area was calculated from the N_2 adsorption isotherm, and the micropore surface area was derived using the *t*-plot method.

Transmission electron microscopy (TEM) was employed to measure particle sizes with TEM JEOL 2010 and TEM JEOL 2100 microscope operating at 200 kV. Size distributions were calculated for each nanoparticle sample by averaging 300 particles from the TEM images.

2.4. Catalytic Tests

Hydrogenation of Levulinic Acid (LA)

In a typical experiment, 2 g of levulinic acid (LA) (98%, Sigma-Aldrich), 0.3 g of a catalyst, and 30 mL of water were combined in a stainless steel autoclave from Berghof, equipped with a Teflon insert allowing a reaction volume of 70 mL. The reactor was pressurized with hydrogen to 50 bar and the temperature was maintained at 30 °C for 1 h.

After the end of the reaction, the reactor was cooled down, the remaining pressure was released, and the reaction mixture was centrifuged to separate the solid catalyst and the product solution. The products were analyzed by HPLC equipped with RID detector and Rezex ROA column, 0.005 N H_2SO_4 was used as an eluent. The liquid after the reaction was analyzed by ICP-MS in order to check the stability of the catalysts.

3. Results and Discussion

3.1. Synthesis and Physicochemical Characterization of the Materials

3.1.1. Synthesis and Composition

In order to compare the different supports, ZrO_2, TiO_2, and mixed oxide ZrO_2–TiO_2 were synthetized by calcination of the alginate gels obtained with the corresponding oxocations. Three different procedures were used to obtain the gels with both cations. The first one involved a co-gelification of the alginate solution in a solution containing the same concentration of Zr^{2+} and Ti^{2+} cations. In the other two procedures an alginate gel was first formed by gelification with either Ti or Zr cations. These cations were then partially exchanged in the presence of a solution of the other cation (Ti or Zr, respectively), allowing a maximum of 50% ion exchange in the alginate gel. The composition

of the resulting oxide depends on the relative affinities of alginate toward Zr or Ti, the values obtained are reported in Table 1 as atomic ratios.

Table 1. Physicochemical properties of the catalysts.

Catalyst	BET [m^2/g]	Total Pore Volume [cm^3/g]	Average Pore Radius [nm]
Ru/ZR-1	100	0.62	11
Ru/ZR-2	127	0.64	9
Ru/ZR-3	125	0.58	9
Ru/TiO$_2$	180	0.69	7
Ru/ZrO$_2$	112	0.61	10

As it is shown in Table 1, the highest surface area was noticed for a catalyst based on titania (180 m^2/g), while for the binary oxides and zirconia, similar surface areas were measured (100–125 m^2/g). The ZrO$_2$–TiO$_2$ samples with a higher surface area also exhibited lower crystallinity (Figure 1). The high surface areas of the binary samples calcined at 450 °C can be assigned to the amorphous nature of these mixed oxides. This might result from additional porosity within highly disordered material and/or from the presence of very small noncrystallized phase exhibiting a consequently higher external surface area. This behavior was also noted in the literature [18].
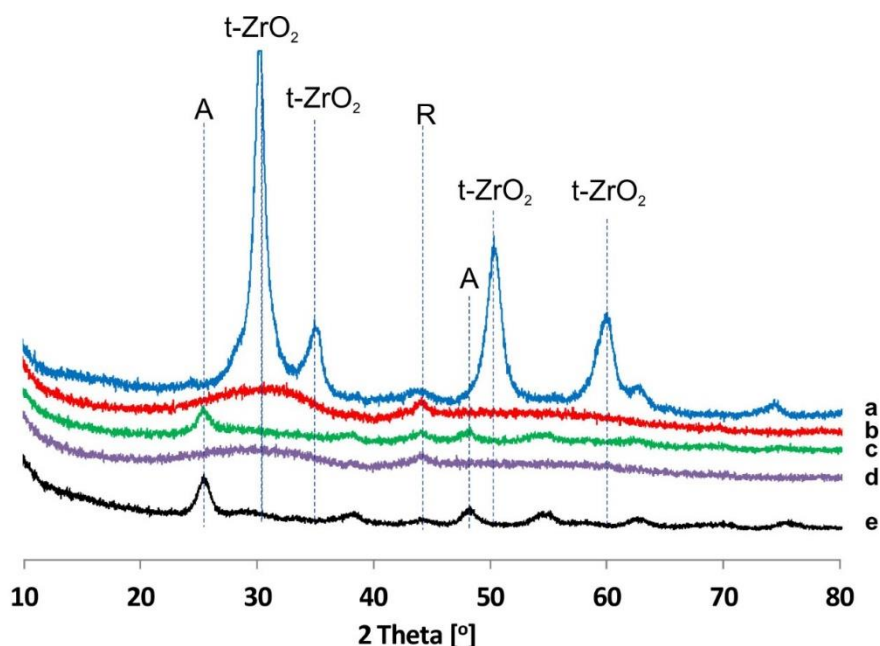

Figure 1. XRD patterns of the ruthenium catalysts. (**a**) Ru/ZrO$_2$; (**b**) Ru/ZR-3; (**c**) Ru/ZR-2; (**d**) Ru/ZR-1; (**e**) Ru/TiO$_2$; R-(Ru JCPDS 00-006-0663); t-ZrO$_2$ JCPDS 00-042-1164; A (a-TiO$_2$ 00-021-1272).

3.1.2. X-Ray Diffraction Tests

X-ray diffraction analysis was also carried out to obtain the structural information of synthesized zirconia, titania, and bioxide systems obtained via the alginate route. Powder wide angle XRD patterns for the studied catalysts are shown in Figure 1.

Generally, the monoxide supports of the catalysts revealed more crystalline structures, whereas the bioxide materials were more amorphous. For the Ru supported on monoxides (Figure 1a,e), the signals at 2θ (29.8°, 33.9°, 50.1°, 59.3°) represent tetragonal zirconia, whereas in the case of titania only the anatase structure was identified (the diffraction peaks at 25.3° and 48.1° corresponding to the (1 0 1) and (2 0 0) crystal planes of anatase were the most intense). In addition, nonresolved diffraction lines attributed to the bulk metallic Ru phase assigned to the Ru (101) were observed at 44.0°. Ru must be

present mostly either in the amorphous form or as very small crystallites as very small broad reflexes were only identified on the XRD patterns of all analyzed catalysts [19]. The binary oxide samples were mostly amorphous. Only in the case of Ru/ZR-2, which contained the highest amount of titania, were signals of anatase visible. According to literature reports, in the case of titania–zirconia binary oxides, the presence of a second oxide can strongly influence the crystallization process, especially if equal amounts of both oxides are present [20,21]. This can result in the increase of the crystallization temperature for bioxide materials by even 350 °C compared to pure ZrO_2 or TiO_2 [22]. It was also reported that crystallization of the amorphous equimolar mixture of both oxides to the $ZrTiO_4$ phase can occur [20,23], regardless of the synthesis method. In our case, however, the temperatures used were too low to induce the formation of such phase.

3.1.3. TEM Images and Ru Particle Size Distributions

Figure 2 shows representative TEM images of Ru-based catalysts, along with the corresponding Ru particle size distributions derived from more than 300 particles. The Ru/TiO_2 material displayed homogeneous and monodispersed TiO_2 crystallites, with a small mean TiO_2 particle size of 8 nm, which stays in agreement with XRD measurements (Figure 2a). By contrast, a fully different morphology was observed for the Ru/ZrO_2 material, with a short-length filamentous or chain-like structure rather than dispersed particles.

Among the ZrO_2–TiO_2-based samples, the material with the highest content of TiO_2, the Ru/Zr-2 catalyst, displayed a morphology close to that of the pure TiO_2-based material, with homogeneously sized oxide crystallites, exhibiting, however slightly, higher agglomeration when compared to pure TiO_2. In the contrary, ZrO_2–TiO_2-based materials with higher zirconia contents, Ru/Zr-1 and Ru/Zr-3 catalysts, exhibited an intermediated morphology, with a less defined structure and the presence of a high amount of amorphous phase, which is in agreement with the results obtained from XRD measurements.

The Ru nanoparticles (NPs') size distribution concerning the two monoxide-supported catalysts differ. The Ru/TiO_2 catalyst displayed a high metal dispersion with a duo-modal particle size distribution and an average particle size centered at 1.9 nm, with a small contribution of larger particles of size around 3.7 nm. Those observations are in agreement with the literature findings where Ru particle size in Ru/TiO_2 is typically less than 2 nm [24,25]. In contrast, for Ru/ZrO_2, much broader distribution with the largest nanoparticle size (5.1 nm) among analyzed catalysts was observed. This value is also comparable to the ones found in the previous reports where the formation of larger Ru crystallites was favorized on zirconia and comparable sizes of NPs (4–6 nm) were identified.

Relatively high dispersion of Ru was reached in the case of bioxide-supported samples possessing a significant contribution of titania. Among them, the smallest Ru NPs were identified for the Ru/ZR-2 sample, which on the histogram were centered around 1.4 nm, and a mono modal distribution was observed. In the case of Ru/ZR-1, although the NPs' size is centered around a slightly higher value (1.7 nm), the advantage is that the larger particles were not observed in this case. The lowest dispersion of Ru among the bioxide catalysts was identified in the amorphous zirconia reach sample Ru/ZR-3, where based on the histogram, we could identify a bimodal-like distribution with particles of 2 nm and a significant contribution of higher diameters centered around 6 nm.
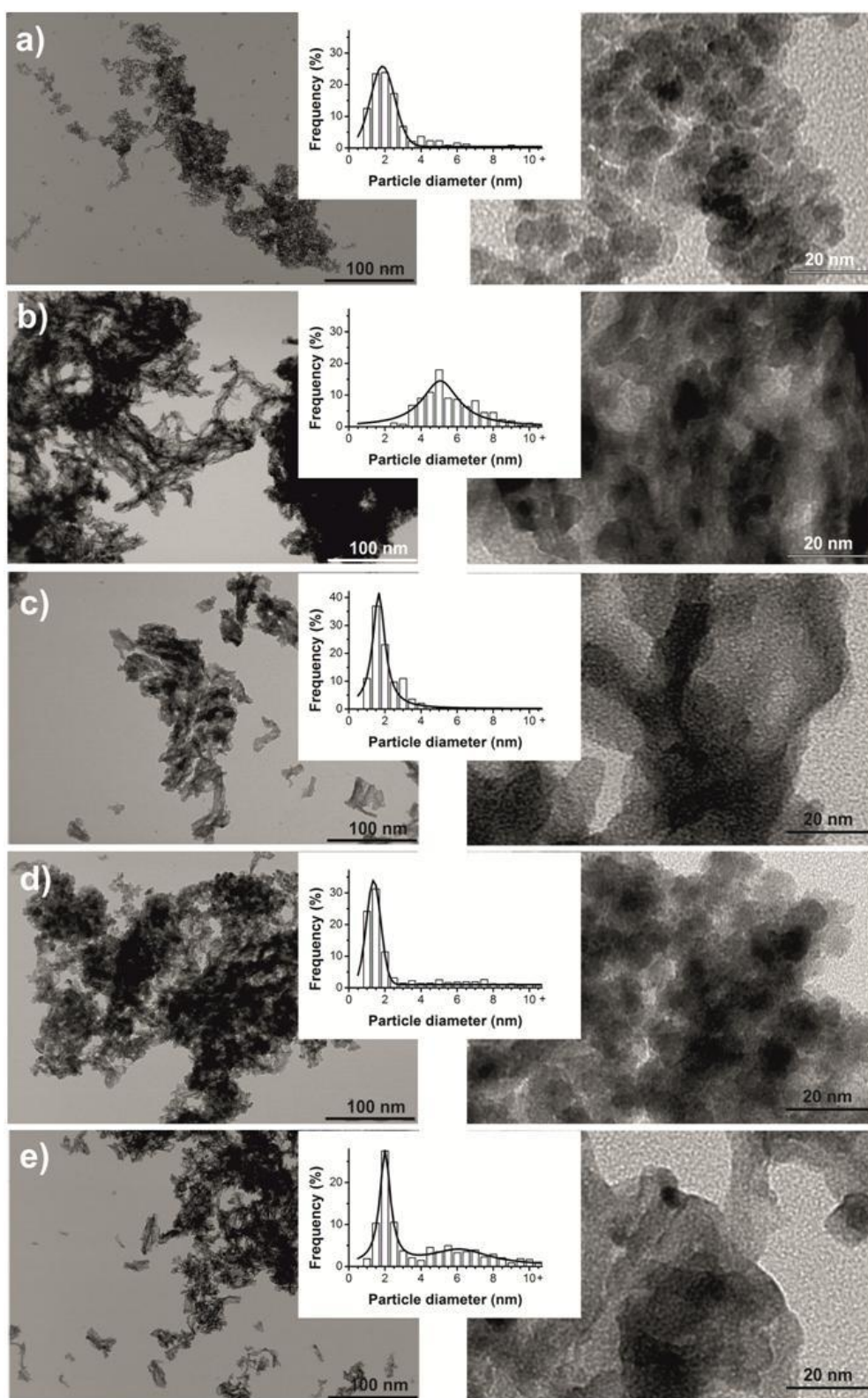
Figure 2. TEM images of Ru catalysts with Ru particle size distribution. (**a**) Ru/TiO_2; (**b**) Ru/ZrO_2; (**c**) Ru/ZR-1; (**d**) Ru/ZR-2; (**e**) Ru/ZR-3.

3.1.4. ToF-SIMS and SEM Study

The SEM-EDS images and ToF-SIMS measurements were obtained in order to study the morphology of the catalysts and compare the distribution of oxides on the surface. Similar morphology

was observed in all the samples and spherical particles were identified in all studied materials by SEM (Figure 3). In the case of Ru/ZrO_2, the structure of this catalyst looks more dense and packed with agglomerations of grains, and less free volume is present, whereas Ru/TiO_2 is more porous. This is in line with the results obtained from the surface area measurements. It is possible to find some similarities among the analyzed catalysts—both Ru/ZR-3 and ZrO_2 resemble the structure of ZrO_2, whereas the remaining two (Ru/ZR-1 and Ru/ZR-2) resemble the titania surface. These findings are in line with previous fundamental results showing that, in the case of heterocationic gels synthesized by cation exchange, the morphology of the gel—and thus the resulting materials—is fixed through the formation of the gel by the first cation [4]. Such structures are similar to those observed in the literature that possess a high surface area [18].
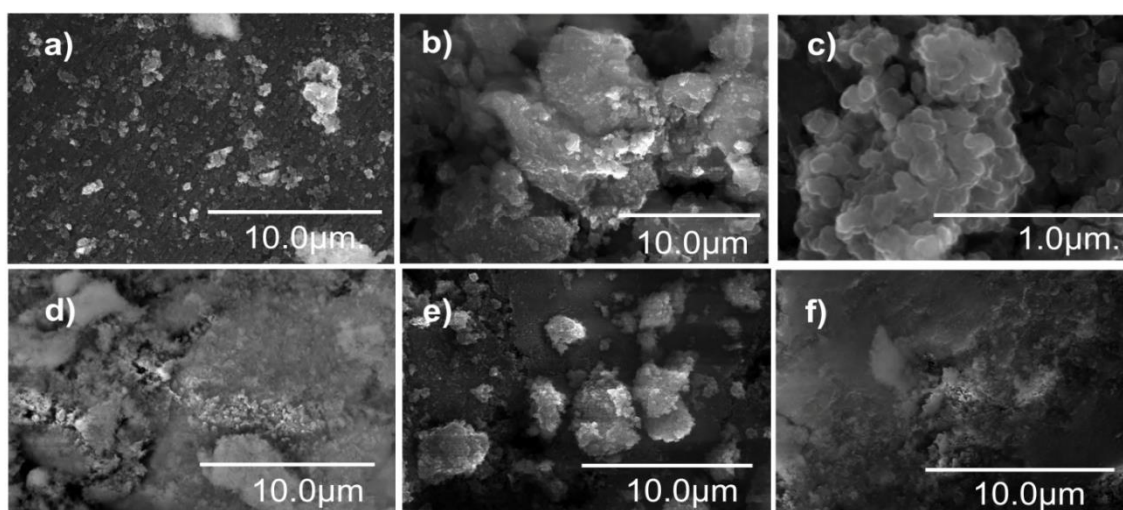

Figure 3. SEM images of Ru catalysts: (**a,c**) Ru/ZrO_2; (**b**) Ru/TiO_2; (**d**) Ru/ZR-1; (**e**) Ru/ZR-2; and (**f**) Ru/ZR-3.

In order to identify the surface composition of the analyzed materials, specially the Zr:Ti ratio, the SEM-EDX and ToF-SIMS measurements were conducted.

As illustrated in Table 2, ToF-SIMS analysis was performed for three binary oxide catalysts prepared by different methods (Ru/ZR-1; Ru/ZR-2; Ru/ZR-3). Thus, we analyzed the intensity of several signals corresponding to the presence of chosen ions (Table 2). The dominant intensity of zirconia on the surface was found in the case of Ru/ZR-3, while the lowest was found for Ru/ZR-2. This correlates with the intensity of the sulfur-containing ion, which was the highest in the case of Ru/ZR-2, where the highest titania surface exposition and the same traces of its precursor were observed. Respectively, the smallest amount of sulfur was noticed in the case of Ru/ZR-3, where the highest exposition of zirconia was observed.

Table 2. Normalized intensity of selected ions calculated on the basis of the ToF-SIMS mass spectra collected from the surface of catalyst and elemental compositions derived from SEM-EDX analysis.

Catalyst	Ion Intensity (ToF-SIMS)				Elemental Composition (SEM-EDX)	
	Zr^+/Ti^+	Cl^-	SO_4^-	Na^+	Zr/Zr+Ti (Atom %)	TiO_2/ZrO_2+TiO_2 (mass %)
Ru/ZR-1	0.32	0.0064	0.0132	0.0034	58	42
Ru/ZR-2	0.034	0.0070	0.0373	0.0028	11.7	82.5
Ru/ZR-3	1.10	0.0057	0.0063	0.0024	85	12
Ru/TiO_2	-	-	-	-	0	100
Ru/ZrO_2	-	-	-	-	100	0

However, in this case it is not possible to determine the exact contribution of each of the components of the support due to the changes in intensities of ToF-SIMS signal noticed for various ions that cannot not be considered proportional. That is why ToF-SIMS gives only information about observed trends and not about the exact composition of the material as with EDX.

SEM-EDX analysis revealed that when an equimolar mixture of both precursors was used in the first step, the obtained material contained almost equal proportions of both oxides with a slight dominance of titania. This shows an almost equal affinity of zirconia and titania for alginate. The synthesis pathway by ion exchange should then lead to almost the same result, which is not at all the case, as for each sample, the first cation used to prepare the initial gel is always highly predominant in the end materials. Indeed, it seems that the first step of the material synthesis is the deciding factor. When zirconia precursor was used to prepare the initial gel beads in the first step, the highest contribution of this oxide was found on the surface (catalyst Ru/ZR-3 with a 85:12 ZrO_2/TiO_2 ratio). In contrast, when titania was used in the first step, it was found to appear in majority (Ru/ZR-2). These results could be explained based on a previous work done on pure ZrO_2 materials synthesized by the alginate route [8]. Indeed, we previously showed that the zirconium chloride precursor forms, in an acidic environment necessary for the gel formation, a stable isolated tetramer $[Zr(OH)_2.4H_2O]_4^{8+}$. In that particular case, the gelation is then probably due to the complexation of the tetramer by the carboxylate groups of the alginate. Such a bulky environment could prevent the diffusion of titania in the polymeric structure when the zirconia-based gel is synthesized first. On the contrary, when titania is used first to form the gel, the bulky tetramer formed by zirconia could prevent its diffusion within the gel bead.

3.1.5. Reducibility of Catalysts by TPR

The reducibility of investigated catalysts was examined by TPR (Figure 4). For Ru/TiO$_2$, we observed the main reduction sharp peak at very low temperatures of around 70 °C, which can be assigned to RuO_2 in the case of very weak or no interaction with the support or amorphous RuO_x. At higher temperatures, the shoulder with maximum at 145 °C can probably be assigned to crystalline, well-dispersed RuO_x in strong interaction with titania [26–28].
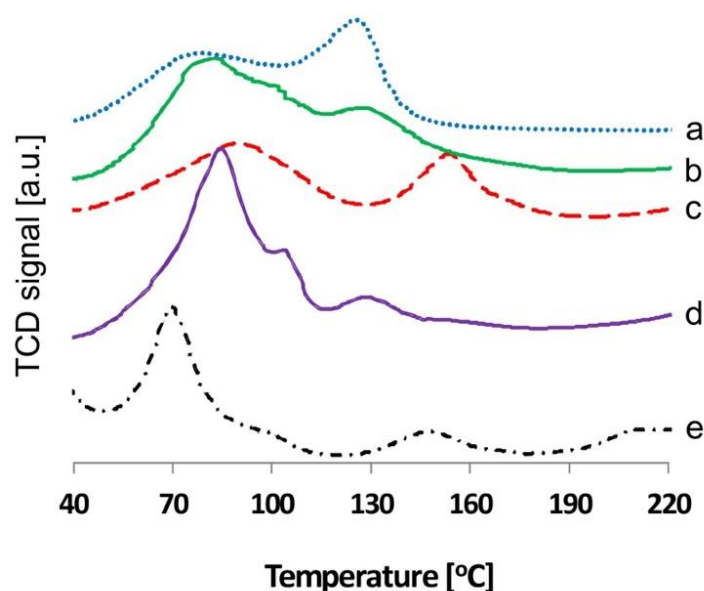

Figure 4. Temperature-programmed reduction profiles of the prepared catalysts; (**a**) Ru/ZrO$_2$, (**b**) Ru/ZR-3, (**c**) Ru/ZR-1; (**d**) Ru/ZR-2; (**e**) Ru/TiO$_2$.

In contrast, Ru/ZrO$_2$ showed the main reduction peak at a high temperature (127 °C), which means that crystalline RuO_x interacting with the support was dominant in this case. The origin of this higher

temperature maximum can be also due to the presence of larger crystallites. There is also a broad, but smaller effect at lower temperature (maximum around 80 °C), which can be related to amorphous RuO_x reduction or ruthenium species of different character, as well as larger crystallites without strong interaction with the support [29].

For binary oxide Ru-supported catalysts, similarly to the case of titania-based materials, low temperature peaks were also identified, however the temperature of the respected maximum hydrogen consumption was shifted towards slightly higher values (80 °C for Ru/ZR-2 to around 90 °C in the case of Ru/ZR-1, respectively). Among those bioxide Ru-supported samples, the Ru/ZR-2 most resembled the Ru/TiO_2, the hydrogen uptake profile was however broader, and in addition to the main peak two small shoulders could be also identified (at 100 and 130 °C). This could suggest that similar Ru species, as for Ru/TiO_2, are present in this case. The Ru/ZR-1 also showed a similar profile, but the low temperature reduction peak was even wilder without a well-defined maximum, similar to the low temperature profile of Ru/ZrO_2. This might suggest the presence of amorphous RuO_x. Additionally, there was quite a significant contribution of the well-defined high temperature maximum (152 °C). This contribution resembled the high temperature effect of Ru/TiO_2 and can be related with the presence of the more crystalline species and more strongly interacting with the support. In the case of Ru/ZR-3 there is very broad peak observed with two maxima (81 °C and 125 °C), which like in previous cases suggests the presence of two different species, most probably the presence of amorphous and crystalline RuO_x respectively [26–28].

3.2. Catalytic Tests

Ru catalysts were used in the model hydrogenation of levulinic acid towards gamma-valerolactone and the results are reported in Table 3. All tested catalysts were active in this reaction and selective towards GVL. The highest activity was observed for Ru/TiO_2, which contained bare titania as a support, followed by Ru/ZR-2, with the highest titania to zirconia ratio among binary oxide catalysts. Activities of the other three catalysts (Ru/ZrO_2, Ru/ZR-3, and Ru/ZR-1) were similar to one another.

Table 3. Catalytic results of levulinic acid hydrogenation towards ɣ-valerolactone.

Catalyst	GVL Yield [%]	LA Conversion [%]
Ru/ZrO_2	32	32
Ru/ZR-1	35	35
Ru/ZR-2	42	42
Ru/ZR-3	30	33
Ru/TiO_2	76	79

The supported ruthenium catalysts were stable in the reaction conditions, since ICP analyses evidenced no leaching of noble metal during the tests. By contrast, the investigated catalysts differed in terms of mechanical stability under the operating conditions. Indeed, whereas pure zirconia and zirconia-rich supports were fully mechanically stable with no change of grain shape occurring during the test, a large fraction of the titania and titania-rich support grains was crushed after the test, with a strong reduction of grain size being observed.

These differences of activity for investigated catalysts can be traced back to the composition of the catalysts, particularly the Zr/Ti ratio on the surface and in the bulk, which is a key factor. Subsequent catalyst properties can directly originate from that. As it was illustrated on the Figure 5, there is a clear relationship between GVL yield and titania contribution. By increasing the titania content reaction, yield is enhanced.
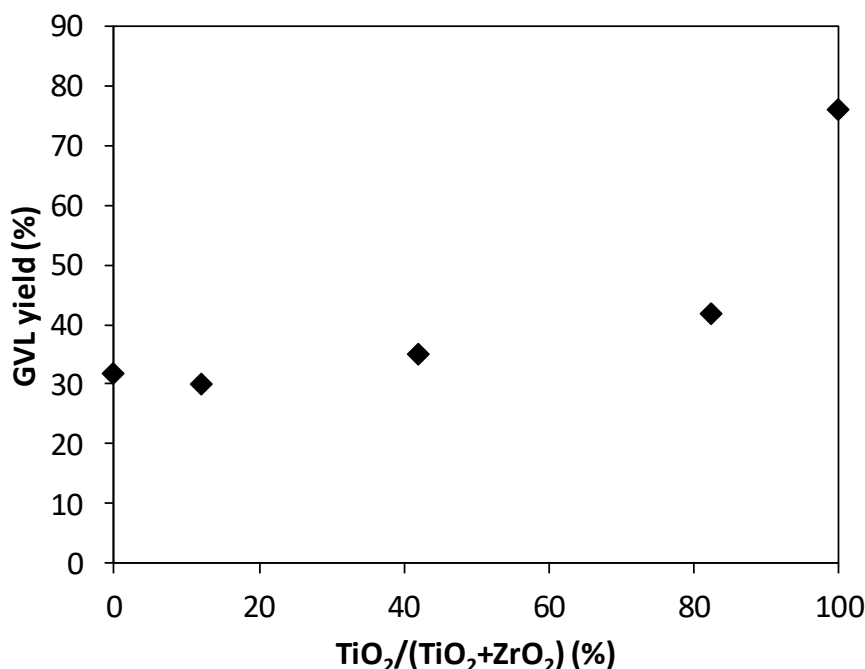
Figure 5. Evolution of ɣ-valerolactone yield vs. TiO$_2$ content in the support.

4. Discussion

Generally, the tendency of the formation of larger metal particles was observed on the zirconia (5.1 nm for Ru/ZrO$_2$), whereas titania and titania-mixed oxides favored formation of smaller NPs (average size not exceeding 2 nm). The particle distribution can also strongly differ for the same material depending on its morphological and physical properties, like presence or type of crystallographic phase [13]. As was shown by us, the highest amount of the Zr in the oxide framework contributed to a lower crystallization degree and therefore highest content of the amorphous phase in a binary oxide. It is known that amorphous oxides differ strongly from their crystalline counterparts e.g., they possess higher concentrations of defects, which can result in a different method for NPs' stronger adhesion of Ru on such anatase phases [18].

Additionally, it is worth mentioning that both zirconia and titania are usually considered as partially reducible supports. Despite being prepared in mild conditions in our case, partial reduction of both oxides cannot be excluded [30]. Generally, titania is known to be a more reducible support than zirconia [4]. According to previous works, the existence of a weak interaction of RuO$_x$ with TiO$_2$ was correlated to the presence of a titania anatase phase of support, as this was notably evidenced by TPR studies where low temperature effects were principal [31].

A similar behavior was observed in the case of titania and titania-rich binary oxide-supported Ru catalysts, for which low temperature effects were strongly dominant, and assigned to small, well dispersed crystallites of RuO$_2$ with very weak or without any interaction with the support. Presumably, there are more active species available at the catalyst surface, as activity in LA hydrogenation was the highest in those two cases.

The difference in the activity of Ru/TiO$_2$ (76% GVL yield) and titania-rich sample Ru/ZR-2 (42% GVL yield) can be related to the presence of the zirconia in the network and the higher contribution of the amorphous phase in the latter case. The modification of the oxide properties directly affects the Ru species' character. Smaller crystallites interacting slightly more strongly with the support were identified in that case. It is probable that too strong an interaction of Ru species gives rise to lower activity.

In the case of zirconia-based materials, it is possible that partial encapsulation and/or decoration can occur during the impregnation and the subsequent temperature-activated reduction of the catalyst,

with formation of Zr^{n+} species at the metal support interface, through the reduction of zirconia in close connection to the metal sites [32]. This was well evidenced by TPR spectra, which suggest the strongest interaction of Ru species with the support.

It was additionally suggested in the literature that the existence of an amorphous zirconia phase close to ruthenium particles can cause the cleavage of Zr–O bonds and the subsequent rearrangement of both the support surface and the crystal lattice. As a result, not only ruthenium is reduced during the reduction step, but also the surrounding ZrO_2 may become partially reduced by hydrogen spilled over from Ru particles [33]. It is therefore worth noting that the sole presence of amorphous phases in the binary oxide materials could amplify the phenomenon of the support partial reduction. This effect would thus be less important for titania-rich binary oxide-supported catalysts. Based on the reduction profiles, one can also assume that ruthenium in binary oxides remains in interaction with both zirconia and titania phases.

This could explain why the Ru supported on zirconia and zirconia-rich binary oxides displayed similar activities, while the activity became higher with further increase of the titania content in the support, from titania-rich binary oxide-supported Ru to zirconia-free Ru/TiO_2 catalyst.

5. Conclusions

We showed a novel way of preparing high surface area mono- and binary oxide materials based on zirconia and titania via the alginate route. They were applied as catalysts for levulinic acid hydro-genation towards γ–valerolactone. The performed investigations revealed that their composition depended on both the nature of the divalent cation and the synthesis conditions. It was demonstrated that the proposed synthesis method allows for modifications of the shape, morphology, and surface properties of these materials. This is especially important taking into account the perspective of their commercialization. The highest amount of Zr in the oxide framework contributes to a lower crystallization degree and, therefore, the highest contribution of the amorphous phase in the binary oxide. The presence of an amorphous phase induces a different character of Ru species. A comparison of the activity in levulinic acid hydrogenation towards γ–valerolactone exhibited that the titania-rich-supported catalyst proved to be the most active, possessing a large surface area anatase phase without any strong interaction with ruthenium.

Conflicts of Interest: The authors declare no conflict of interest.

References

1.　Fu, X.; Clark, L.A.; Yang, Q.; Anderson, M.A. Enhanced photocatalytic performance of titania-based binary metal oxides: TiO_2/SiO_2 and TiO_2/ZrO_2. *Environ. Sci. Technol.* **1996**, *30*, 647–653. [CrossRef]

2.　Quignard, F.; Valentin, R.; Di Renzo, F. Aerogel materials from marine polysaccharides. *New J. Chem.* **2008**, *32*, 1300–1310. [CrossRef]

3.　Horga, R.; Di Renzo, F.; Quignard, F. Ionotropic alginate aerogels as precursors of dispersed oxide phases. *Appl. Catal. A* **2007**, *325*, 251–255. [CrossRef]

4.　Agulhon, P.; Robitzer, M.; David, L.; Quignard, F. Structural regime identification in ionotropic alginate gels: Influence of the cation nature and alginate structure. *Biomacromolecules* **2012**, *13*, 215–220. [CrossRef]

5.　Monakhova, Y.; Agulhon, P.; Quignard, F.; Tanchoux, N.; Tichit, D. New mixed lanthanum- and alkaline-earth cation-containing basic catalysts obtained by an alginate route. *Catal. Today* **2012**, *189*, 28–34. [CrossRef]

6.　Behar, S.; Gonzalez, P.; Agulhon, P.; Quignard, F.; Swierczynski, D. New synthesis of nanosized Cu–Mn spinels as efficient oxidation catalysts. *Catal. Today* **2012**, *189*, 35–41. [CrossRef]

7. Agulhon, P.; Constant, S.; Chiche, B.; Lartigue, L.; Larionova, J.; Di Renzo, F.; Quignard, F. Controlled synthesis from alginate gels of cobalt–manganese mixed oxide nanocrystals with peculiar magnetic properties. *Catal. Today* **2012**, *189*, 49–54. [CrossRef]

8. Wan, E.; Travert, A.; Quignard, F.; Tichit, D.; Tanchoux, N.; Petitjean, H. Modulating properties of pure ZrO_2 for structure–activity relationships in acid-base catalysis: Contribution of the alginate preparation route. *ChemCatChem* **2017**, *9*, 2358–2365. [CrossRef]

9. Michel, C.; Zaffran, J.; Ruppert, A.M.; Matras-Michalska, J.; Jedrzejczyk, M.; Grams, J.; Sautet, P. Role of water in metal catalyst performance for ketone hydrogenation: A joint experimental and theoretical study on levulinic acid conversion into gamma-valerolactone. *Chem. Commun.* **2014**, *50*, 12450–12453. [CrossRef]

10. Al-Shaal, M.G.; Wright, W.R.H.; Palkovits, R. Exploring the ruthenium catalysed synthesis of γ-valerolactone in alcohols and utilisation of mild solvent-free reaction conditions. *Green Chem.* **2012**, *14*, 1260–1263. [CrossRef]

11. Tan, J.; Cui, J.; Deng, T.; Cui, X.; Ding, G.; Zhu, Y.; Li, Y. Water-promoted hydrogenation of levulinic acid to γ-valerolactone on supported ruthenium catalyst. *ChemCatChem* **2015**, *7*, 508–512. [CrossRef]

12. Piskun, A.; Winkelman, J.M.G.; Tang, Z.; Heeres, H.J. Support screening studies on the hydrogenation of levulinic acid to γ-valerolactone in water using Ru catalysts. *Catalysts* **2016**, *6*, 131. [CrossRef]

13. Ruppert, A.M.; Grams, J.; Jedrzejczyk, M.; Matras-Michalska, J.; Keller, N.; Ostojska, K.; Sautet, P. Titania-supported catalysts for levulinic acid hydrogenation: Influence of support and its impact on γ-valerolactone yield. *ChemSusChem* **2015**, *8*, 1538–1547. [CrossRef]

14. Ftouni, J.; Muñoz-Murillo, A.; Goryachev, A.; Hofmann, J.P.; Hensen, E.J.M.; Lu, L.; Kiely, C.J.; Bruijnincx, P.C.A.; Weckhuysen, B.M. ZrO_2 is preferred over TiO_2 as support for the Ru-catalyzed hydrogenation of levulinic acid to γ-valerolactone. *ACS Catal.* **2016**, *6*, 5462–5472. [CrossRef]

15. Genuino, H.C.; Bruijnincx, P.C.A.; Weckhuysen, B.M. Influence of sulfuric acid on the performance of Ruthenium-based catalysts in the liquid-phase hydrogenation of levulinic acid to γ-valerolactone. *ChemSusChem* **2017**, *10*, 2891–2896.

16. Ruppert, A.M.; Grams, J.; Matras-Michalska, J.; Chełmicka, M.; Przybysz, P. ToF-SIMS study of the surface of catalysts used in biomass valorization. *Surf. Interface Anal.* **2014**, *46*, 726–730. [CrossRef]

17. Wachała, M.; Grams, J.; Kwapiński, W.; Ruppert, A.M. Influence of ZrO_2 on catalytic performance of Ru catalyst in hydrolytic hydrogenation of cellulose towards γ-valerolactone. *Int. J. Hydrogen Energ.* **2016**, *41*, 8688–8695. [CrossRef]

18. Zhang, H.; Chen, B.; Banfield, J.F.; Waychunas, G.A. Atomic structure of nanometer-sized amorphous TiO_2. *Phys. Rev. B* **2008**, *78*, 214106. [CrossRef]

19. Leo, I.M.; Granados, M.L.; Garcia Fierro, J.L.; Mariscal, R. Sorbitol hydrogenolysis to glycols by supported ruthenium catalysts. *Chin. J. Catal.* **2014**, *35*, 614–621. [CrossRef]

20. Zou, H.; Lin, Y.S. Structural and surface chemical properties of sol–gel derived TiO_2–ZrO_2 oxides. *Appl. Catal. A* **2004**, *265*, 35–42. [CrossRef]

21. Perez-Hernandez, R.; Mendoza-Anaya, D.; Fernandez, M.E.; Gomez-Cortes, A. Synthesis of mixed ZrO_2–TiO_2 oxides by sol–gel: Microstructural characterization and infrared spectroscopy studies of NO_x. *J. Mol. Catal. A* **2008**, *281*, 200–206. [CrossRef]

22. Sohn, J.R.; Lee, S.H. Effect of TiO_2–ZrO_2 composition on catalytic activity of supported $NiSO_4$ for ethylene dimerization. *Appl. Catal. A* **2007**, *321*, 27–34. [CrossRef]

23. Xu, Q.; Anderson, M.A. Sol–gel route to synthesis of microporous ceramic membranes: Thermal stability of TiO_2–ZrO_2 mixed oxides. *J. Am. Ceram. Soc.* **1993**, *76*, 2093–2097. [CrossRef]

24. Triki, M.; Minh, D.P.; Ksibi, Z.; Ghorbel, A.; Besson, M. Ruthenium catalysts supported on TiO_2 prepared by sol–gel way for *p*-hydroxybenzoic acid wet air oxidation. *J. Sol-Gel Sci. Technol.* **2008**, *48*, 344–349. [CrossRef]

25. Mori, K.; Miyawaki, K.; Yamashita, H. Ru and Ru–Ni nanoparticles on TiO_2 support as extremely active catalysts for hydrogen production from ammonia–borane. *ACS Catal.* **2016**, *6*, 3128–3135. [CrossRef]

26. Liu, X.; Zeng, J.; Shi, W.; Wang, J.; Zhu, T.; Chen, Y. Catalytic oxidation of benzene over ruthenium–cobalt bimetallic catalysts and study of its mechanism. *Catal. Sci. Technol.* **2017**, *7*, 213–221. [CrossRef]

27. Debecker, D.P.; Farin, B.; Gaigneaux, E.M.; Sanchez, C.; Sassoye, C. Total oxidation of propane with a nano-RuO_2/TiO_2 catalyst. *Appl. Catal. A* **2014**, *481*, 11–18. [CrossRef]

28. Li, L.; Qu, L.; Cheng, J.; Li, J.; Hao, Z. Oxidation of nitric oxide to nitrogen dioxide over Ru catalysts. *Appl. Catal. B* **2009**, *88*, 224–231. [CrossRef]

29.　Bi, J.-L.; Hong, Y.-Y.; Lee, C.-C.; Yeh, C.-T.; Wang, C.-B. Novel zirconia-supported catalysts for low-temperature oxidative steam reforming of ethanol. *Catal. Today* **2007**, *129*, 322–329. [CrossRef]

30.　Hadjiivanov, K.; Lavalley, J.-C.; Lamotte, J.; Mauge, F.; Saint-Just, J.; Che, M. FTIR study of CO interaction with Ru/TiO$_2$ catalysts. *J. Catal.* **1998**, *176*, 415–425. [CrossRef]

31.　Gonzalez Carballo, J.M.; Finocchio, E.; Garcia, S.; Rojas, S.; Ojeda, M.; Busca, G.; Garcia Fierro, J.L. Support effects on the structure and performance of ruthenium catalysts for the Fischer–Tropsch synthesis. *Catal. Sci. Technol.* **2011**, *1*, 1013–1023. [CrossRef]

32.　Álvarez-Rodríguez, J.; Rodríguez-Ramos, I.; Guerrero-Ruiz, A.; Gallegos-Suarez, E.; Arcoya, A. Influence of the nature of support on Ru-supported catalysts for selective hydrogenation of citral. *Chem. Eng. J.* **2012**, *204–206*, 169–178.

33.　Coq, B.; Kumbhar, P.S.; Moreau, C.; Moreau, P.; Figueras, F. Zirconia-supported monometallic Ru and bimetallic Ru-Sn, Ru-Fe catalysts: Role of metal support interaction in the hydrogenation of cinnamaldehyde. *J. Phys. Chem.* **1994**, *98*, 10180–10188. [CrossRef]